## Author's Version

# Investigation of CMAS Resistance of Sacrificial Suspension Sprayed Alumina Topcoats on EB-PVD 7YSZ Layers

**by**

**Christoph Mikulla[1], Ravisankar Naraparaju[1], Uwe Schulz[1], Filofteia-Laura Toma[2], Maria Barbosa[2,3], Christoph Leyens[2,3]**

[1)] German Aerospace Center (DLR), Institute of Materials Research, Cologne, Germany
[2)] Fraunhofer Institute for Material and Beam Technology (IWS), Dresden, Germany
[3)] Technische Universität Dresden (TUD), Institute of Materials Science, Dresden, Germany

Proceedings of the International Thermal Spray Conference and Exposition (ITSC 2019) p.79-85
May 26-29, 2019
Yokohama, Japan

ISBN: 9781510888005
ASM International
*http://www.proceedings.com/49258.html*

# *Investigation of CMAS Resistance of Sacrificial Suspension Sprayed Alumina Topcoats on EB-PVD 7YSZ Layers*

***Christoph Mikulla*, Ravisankar Naraparaju, Uwe Schulz***
*German Aerospace Center (DLR), Institute of Materials Research, Cologne, Germany*
*) christoph.mikulla@dlr.de

***Filofteia-Laura Toma[1,]*, Maria Barbosa[1,2], Christoph Leyens[1,2]***
[1)] *Fraunhofer Institute for Material and Beam Technology (IWS), Dresden, Germany*
[2)] *Technical University of Dresden (TUD), Institute of Materials Science, Dresden, Germany*
*) filofteia-laura.toma@iws.fraunhofer.de

## Abstract

Molten calcium-magnesium-aluminum-silicate (CMAS) mineral particles cause significant degradation of thermal barrier coatings (TBCs) in aero-engines. One approach to protect the TBC coating against the CMAS attack is the application of a sacrificial coating on top of the TBC coating. In this work sacrificial $Al_2O_3$ coatings were deposited on top of EB-PVD 7YSZ layers using suspension thermal spraying starting from an aqueous $Al_2O_3$ suspension. Spray parameters were varied in order to produce sacrificial topcoats with two different microstructures and porosities levels. The coating systems were tested under CMAS attack by performing short- and long-time infiltration tests at 1250 °C. It was found out that the porosity and morphology of $Al_2O_3$ coatings strongly influenced the CMAS infiltration kinetics and the formation of various phases. CMAS mitigation depended on the interaction between the coating morphology which rules the driving force for infiltration, as well as on the reaction speed between alumina and the CMAS deposit.

## Introduction

In modern airplane engines and gas turbines, thermal barrier coatings (TBCs) are deposited on various components (like turbine blades, vanes, combustion liners) in the high temperature section, in order to increase the operating temperature and hence to improve the efficiency and power of the engine. 7 wt.-% $Y_2O_3$ stabilized $ZrO_2$ (7YSZ) ceramic is used as state-of-the-art TBC material [1-3]. It is typically deposited either by electron beam physical vapor deposition (EB-PVD) or by atmospheric plasma spraying (APS) [4]. These processes create a porous microstructure with low thermal conductivity and high resistance against thermal cyclic stresses that occur due to thermal expansion. In operating conditions, the TBC coatings undergo severe degradation by interaction with molten calcium-magnesium-aluminum-silicate (CMAS) minerals that are typically found in desert sands or volcanic ashes [5-7]. After infiltration of the CMAS into the porous coating, chemical reactions and phase transformations can cause residual stresses, cracks and spallation, strongly reducing the life-time of the component. The state-of-the art TBC material 7YSZ offers only limited resistance to the CMAS attack. Intense research has been and still is done in the last decades to solve this issue.

One strategy is the deposition of a sacrificial layer on top of the TBC. The sacrificial layer has to dispose a high reactivity with the molten CMAS and to form crystalline phases that delay further infiltration by sealing pores and gaps of the TBC [8-10]. Aluminum oxide ($Al_2O_3$) is a promising candidate as sacrificial top-layer, due to the formation of arresting phases which offer a good CMAS resistance. Alumina has already been deposited as a CMAS resistant material on top of 7YSZ with different deposition techniques [11-13]. The most recent study was published by Naraparaju et al. [14], who deposited the alumina topcoat using EB-PVD technology. However, EB-PVD $Al_2O_3$-topcoats suffered locally from cracks that arise from crystallization and sintering shrinkage. As a consequence, the resistance against CMAS infiltration was insufficient due to the characteristic morphology. It has been found that the microstructure, the coating density and the distribution of the porosity were critical factors for the efficiency of sacrificial layers against CMAS infiltration and degradation.

As the $Al_2O_3$ layer microstructure is strongly influenced by the fabrication process, new innovative coating methods are used to create the sacrificial layer with the desired morphology. Over the last years, extensive development efforts have uncovered the potential of thermal spraying with suspensions. Coating thicknesses, morphologies and properties can be varied over an extremely wide range, as presented i.e. [15-17]. Direct processing of nano- and sub-micon-sized powders is possible with suspensions, but more important is the advantage of directly using the finely dispersed ceramic oxide powders of widely varying grain size, purity, etc. currently used in the preparation of sintered technical ceramics. Suspensions can be used as feedstock for both atmospheric plasma spraying (APS) and high velocity oxy-fuel spraying (HVOF) processes.
In this work, alumina coatings were sprayed on top of EB-PVD 7YSZ TBCs layers using suspension spraying processes - suspension plasma spraying (SPS) and suspension high velocity oxy-fuel spraying (SHVOF), respectively - starting from an finely dispersed aqueous $Al_2O_3$ suspension. In order

to evaluate the CMAS resistance of the sacrificial $Al_2O_3$ suspension sprayed coatings, short- and long-term isothermal CMAS infiltration tests were performed on the coating systems. Coating microstructure, infiltration kinetics and formed reaction products were investigated by means of scanning electron microscopy, EDX-spectroscopy and X-ray diffraction. The potential of the suspension spraying to produce CMAS-resistant sacrificial $Al_2O_3$ coatings will be presented.

## Experimental Methods

**Preparation of EB-PVD 7YSZ Layers**

7YSZ layers (7wt.-% $Y_2O_3$ stabilized $ZrO_2$) were deposited via EB-PVD (electron beam physical vapor deposition) process at Germany Aerospace Center (DLR) in Cologne, Germany. The coating process used single source evaporation with a 7YSZ ingot. The main process parameters and layer thicknesses are shown in Table 1.

*Table 1: Processing parameters of 7YSZ layers deposited by EB-PVD on $Al_2O_3$ substrates.*

| | **7YSZ for SPS $Al_2O_3$** | **7YSZ for SHVOF$Al_2O_3$** |
|---|---|---|
| Substrate temperature | 860 – 890 °C | 915 - 930 °C |
| Pressure | $6x10^{-3}$ mbar | |
| Rotation speed | 30 rpm | |
| Beam power | 65 kW | |
| Coating thickness | 220 µm | 400 µm |

In order to avoid the oxidation of metal substrates during the infiltration experiments at 1250 °C, the 7YSZ was deposited on flat, 1 mm thick sintered $Al_2O_3$ substrates. Samples with two different 7YSZ-thicknesses of ~ 220 µm and ~ 400 µm were prepared for this study. This thickness deviation of YSZ would not have any significant effect on the results presented here, since this work focuses only on the microstructure and infiltration/reaction kinetics of the sacrificial alumina top layer and not of the underlying 7YSZ-layer.

**Suspension Spraying of Sacrificial $Al_2O_3$ Coatings on YSZ EB-PVD Layers**

Sacrificial alumina sprayed coatings with different microstructures were produced via suspension spraying at Fraunhofer IWS, Dresden, Germany. Suspension-HVOF spraying (SHVOF) was used to produce dense alumina coatings, whereas suspension-APS (SPS) was used to produce rather porous sprayed coatings on top of YSZ EB-PVD layers. A commercially available $Al_2O_3$ raw powder (Martinswerk, Germany) with average particle size ($d_{50}$) of 2.2 µm was used to obtain an aqueous suspension with 25 wt.-% solid content. The suspensions were fed using the industrially suitable three pressurized-vessels suspension feeder developed by Fraunhofer IWS [16-18].

$Al_2O_3$ suspension was internally injected in the modified combustion chamber of a HVOF Top Gun torch (8 mm-diameter and 135 mm-length nozzle, GTV mbh, Germany) using ethylene as fuel gas. In the SPS process, $Al_2O_3$ suspension was externally injected in an APS F6 plasma gun (GTV) with 6 mm-nozzle and $Ar/H_2$ plasma gas mixture. Suspension sprayed coatings with thicknesses of 80 – 90 µm were deposited directly on the top of the EB-PVD YSZ layers.

**CMAS Deposit and Infiltration Experiments**

A CMAS powder was artificially synthetized in the laboratory as described in previous studies [5]. Therefore, Me-nitrates (Me: Al, Ca, Mg, Fe), $SiO_2$ and $TiO_2$ powders (Merck, Germany) were synthesized by means of co-decomposition, followed by a heat treatment at 1250°C for 1 h and then mixing with anhydrite $CaSO_4$ powder at room temperature. The synthetized CMAS powder has a chemical composition of 37.3 mol.-% $SiO_2$, 32.4 mol.-% CaO, 9.9 mol.-% $Al_2O_3$, 11.2 mol.-% MgO, 7.8 mol.-% FeO and 1.4 mol.-%. The CMAS consists of crystalline phases of pyroxene and melilite. Its melting range was found to be between 1215 – 1245 °C and its viscosity log η @ 1250°C of about -0.69 Pa·s.

Infiltration tests were performed by applying CMAS powder with a concentration of 10 mg/cm² on top of the $Al_2O_3$-7YSZ double layer coating system. The samples were heated up to 1250 °C and hold in ambient air isothermally at this temperature for a short duration of 5 min and a long duration of 5 hours, respectively. The short-term infiltration was performed in a cyclic furnace with an overall heating rate of 142 K/min and rapid cooling (quenching) to room temperature with ventilated ambient air. The long-term infiltration was performed in a Netzsch box furnace with a heating and low cooling rate of 10 K/min.

$Al_2O_3$ raw powder used for the development of the aqueous for spraying was mixed with CMAS deposit, in proportion 60 wt. % CMAS deposit, 40 wt. % $Al_2O_3$ and annealed for 5h on a platinum foil allowing the same reaction time as for the coatings.

**Characterization Methods**

The coatings were metallographically prepared and analyzed by scanning electron microscopy (SEM) (DSM ultra 55, Carl Zeiss, Germany).

Energy-dispersive spectroscopy (EDS) (Inca, Oxford Instruments, UK) was used to identify the CMAS reaction products within the coatings. The in-plane porosity of the as-deposited alumina coatings was determined by image analysis in SEM micrographs using the ImageJ software.

XRD analysis of the CMAS-alumina reaction products in powder mixture, as well as of the as-sprayed SPS- and SHVOF-alumina coatings were carried out with a D8 Advance diffractometer with Cu-Kα radiation (Bruker AXS, Germany). By using a powder mixture, a higher quantity of reaction products is formed (due to the higher specific contact surface area) leading to a stronger signal of the relevant peaks.

## Results and Discussion

**Microstructures of the As-Sprayed Suspension Sprayed $Al_2O_3$ Coatings**

Suspension sprayed alumina coatings with different microstructures were successfully deposited on columnar EB-PVD 7YSZ TBCs. The SEM micrographs of as-sprayed coatings at two different magnifications are shown in Fig. 1.

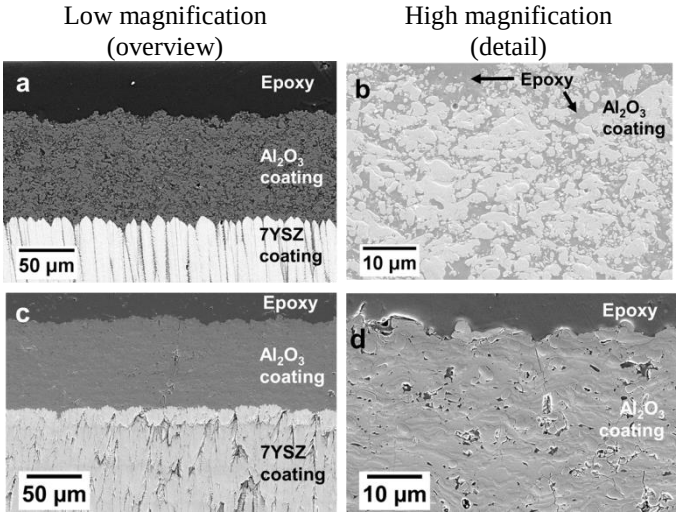


*Figure 1: SEM cross-section micrographs at two different magnifications of as-sprayed SPS-alumina (a, b) and SHVOF-alumina (c, d) on top of EB-PVD 7YSZ TBC.*

The microstructures of the underlying EB-PVD 7YSZ layers have been studied elsewhere [6, 7] and are not specifically investigated in this work. SPS-alumina coating contained a porous microstructure of well-molten particles alternating with partially molten or already cooled finely particles (Figs. 1a and 1b). The porosity of SPS coatings was estimated at around 30 %. SHVOF-alumina coatings were densely structured and contained mostly well-molten particles (Figs. 1c and 1d). The presence of localized vertical cracks coming from the internal/relaxing stresses could be observed in the coating cross-sections. The porosity of SHVOF coatings was estimated of about 4 %.

**Microstructures of the CMAS-Infiltrated Suspension Sprayed $Al_2O_3$ Coatings**

Short-Term Infiltration (5 min @ 1250 °C):

The SEM cross-section micrographs of the alumina coatings after short-term infiltration are shown in Fig. 2. The SPS-alumina coating (Figs. 2a and 2b) is widely infiltrated until the subjacent 7YSZ-layer; furthermore, the infiltration is mostly inhomogeneous. The infiltration depth varies between a few 10 µm up to the entire 90 µm thick alumina coating as shown in the micrograph by the dashed line.

Reduced CMAS infiltration was observed in the SHVOF alumina coating (Fig. 2c and 2d). The molten CMAS deposit has infiltrated only up to a few microns deep. In a few areas where large cracks or gaps were presented, a limited infiltration could be locally observed (light grey areas).

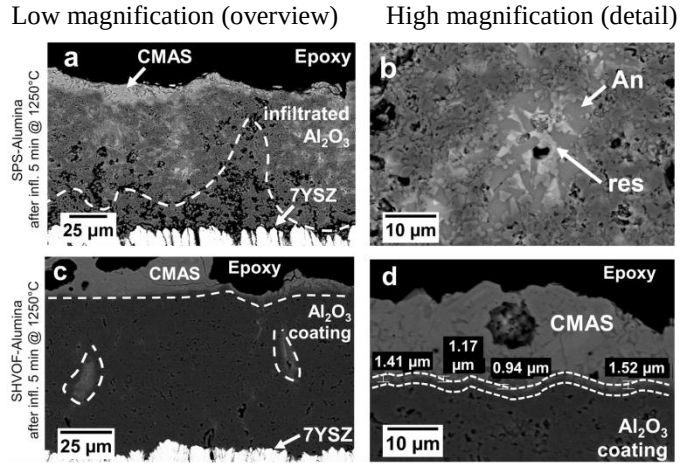


*Figure 2: SEM cross-section micrographs at two different magnifications of the suspension spayed coatings after short-term CMAS infiltration (5 min @ 1250 °C): SPS-alumina (a, b) and SHVOF-alumina (c, d). Dashed lines indicate the infiltration depth; dotted lines indicate the reaction layer. Phases: An= anorthite, CMAS =CMAS/residue*

Long-Term Infiltration (5 h @ 1250 °C):

The SEM-micrographs after long-term infiltration are shown in Fig. 3. The SPS-coating was almost completely infiltrated (Fig. 3a), which allowed the CMAS melt to infiltrate further into the subjacent 7YSZ-layer (Fig. 4a). As shown in the high-magnification micrograph of the Fig. 3b, the resulted reaction products are not offering any resistance to the CMAS infiltration.

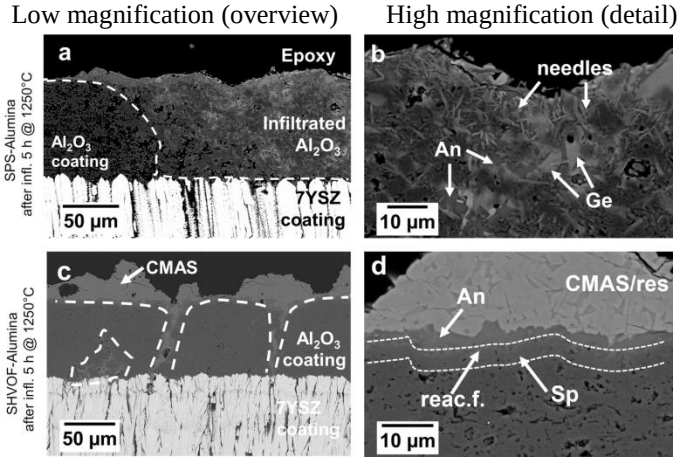


*Figure 3: SEM cross-section micrographs at two different magnifications of the suspension spayed coatings after long-term CMAS infiltration (5 h @ 1250 °C): SPS-alumina (a, b) and SHVOF-alumina (c, d). Dashed lines indicate the infiltration depth; dotted lines indicate the reaction layer. Phases: An = anorthite, Ge = gehlenite, needles = "needle-like" phase, Sp = spinel, reac.f. =reaction front, CMAS =CMAS/ residue*

There is no formation of continuous dense layer; contrary, some phases with a needle-like structure were formed, where the molten CMAS can easily penetrate (Fig. 4a).

In contrast, the SHVOF-coatings have offered much higher resistance to the CMAS flow (Figs. 3c and 3d). The crack-free areas were infiltrated only few µm. Figure 3d shows a high magnification SEM-micrograph of the infiltrated surface. The alumina is slightly infiltrated and formed reaction layer that hindered the CMAS from further infiltration. In the regions of vertical cracks CMAS has infiltrated deeply, reaching the surface of the 7YSZ-layer (Fig. 4b). Moreover, a local dissolution of the coating and formation of new reaction products at the crack interface were observed. These new products induced a broadening of the crack gap, too.

Figure 4 shows SEM micrographs of the 7YSZ/alumina substrate interface and the 7YSZ columnar tips at the $Al_2O_3$/YSZ substrate interface after 5 h infiltration. With fully infiltrated SPS alumina topcoat, the inter-columnar gaps of the 7YSZ were also infiltrated with CMAS; moreover the columns under the SPS-$Al_2O_3$ were detached from the substrate by the CMAS dissolving in to the alumina of the substrate (Fig. 4a). This phenomenon was discussed previously by Naraparaju et al. [6]. Figure 4b shows the infiltrated upper part of 7YSZ columns lying under infiltrated $Al_2O_3$ coating. Both the inter- and intra-columnar gaps of the 7YSZ were found to be infiltrated with CMAS. The column tips of the 7YSZ partly reacted with CMAS; losing the most of their original structure and forming a phase with globular shapes [6]. Since the focus of this study is the sacrificial coating, this reaction of the 7YSZ is not further studied and discussed.

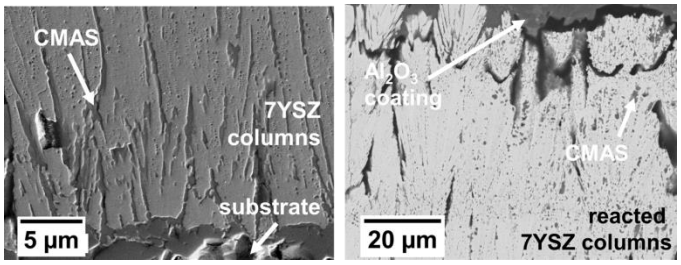


*Figure 4: (a) Infiltrated 7YSZ columns under a SPS-coating at the substrate interface (b) infiltrated and partly reacted 7YSZ column tips located under a crack in the SHVOF-coating. Both after CMAS infiltration 5 h @ 1250°C.*

**Infiltration Behavior SPS vs. SHVOF $Al_2O_3$ Coatings**

The EDS mapping (calcium element) of selected infiltrated coating microstructures is given for comparison purposes in Fig. 5. SPS alumina has been completely infiltrated, the presence of calcium within the YSZ-layer confirming this affirmation (Fig. 5a). Moreover the infiltration was highly inhomogeneous across the coatings. In the case of SHVOF coatings, CMAS infiltration could be identified only in the cracked regions of the coating.

The porosity of the alumina coating has played key role on the CMAS infiltration kinetics. The highly porous SPS-coating (~30%) is infiltrated faster than the dense SHVOF coating (~4%) and undergoes a vigorous reaction allowing the formation of different products. Since the porosity in the SPS-coating was discontinuous and irregular, the infiltration was, par consequence, inhomogeneous.

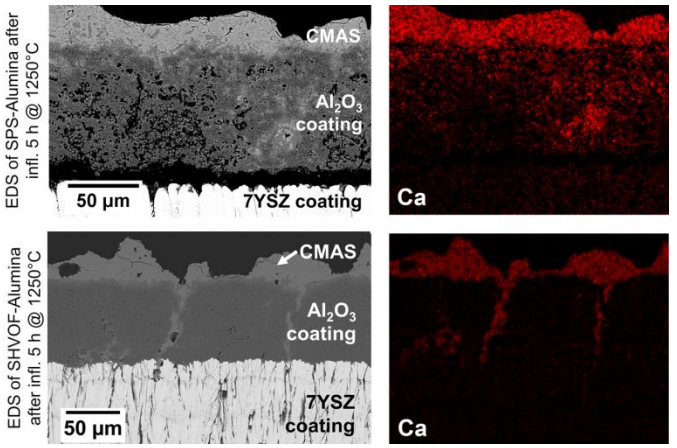


*Figure 5: SEM-micrographs and corresponding EDS mapping (calcium element, red) for infiltrated SPS-alumina coating after 5 min @ 1250 °C (upside) and SHVOF-alumina coating after 5 h @ 1250 °C (downside).*

Nevertheless, the presence of cracks in the SHVOF coating allowed the CMAS infiltration in the YSZ located under the crack region (Fig. 4b), which can be detrimental for the coating resistance.

**Phase Compositions in the $Al_2O_3$-CMAS powder mixtures and as-sprayed $Al_2O_3$-coatings**

The XRD pattern of the $Al_2O_3$-CMAS (40 / 60 wt.-%) powder mixture after 5 h-annealing at 1250 °C as well as the as-sprayed SPS- and SHOVF-$Al_2O_3$ coatings are given in Fig. 6. For the as-sprayed SPS- and SHVOF-$Al_2O_3$ coating, corundum α-$Al_2O_3$ (α) and γ-$Al_2O_3$ peaks (γ) can be assigned. For the powder mixture, the peaks were identified as anorthite (An) $CaAl_2Si_2O_8$, spinel (Sp) $Mg_{1-x}Al_2Fe_xO_4$, gehlenite (Ge) $Ca_2Al_2SiO_7$ and diopside (Dio) $Ca(Mg, Al)(Si, Al)_2O_6$. Additionally, smaller peaks are identified as corundum α-$Al_2O_3$ (α). These findings are in good agreement with those published elsewhere [14]. Since a smaller amount of material was used during XRD-analysis. The original signals for the powder mixture are weaker than for the as-sprayed coatings due to the smaller amount of material used during the XRD-analysis. As a consequence, the peak highs in Fig.6 have been normalized to allow a better identification of the peaks.

Contrary to our previous work [14], peaks of the gehlenite phase could be found here. The formation of gehlenite phase can be explained considering the ternary phase diagram of $AlO_{3/2}$-$SiO_2$-CaO at an isothermal cut of 1300 °C (Fig. 7). The CMAS compositions used in this study (red circle) and CMAS composition used in the previous work (blue triangle) are marked in the phase diagram by using the normalized $Al_2O_3$-$SiO_2$-CaO fractions of the two CMAS while eliminating FeO, MgO and $TiO_2$ fractions. During the infiltration, the CMAS

melt was enriched with $Al_2O_3$, moving the CMAS compositions along the arrows towards the alumina.

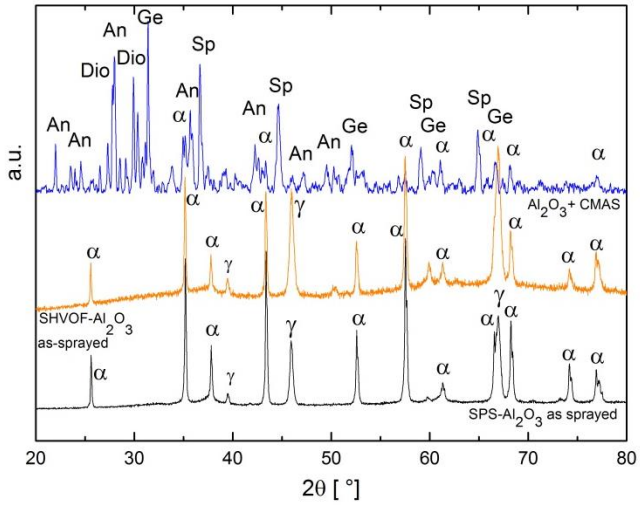


*Figure 6: Normalized XRD pattern of $Al_2O_3$ – CMAS (40 wt. % - 60 wt. %) powder mixture after 5 h-annealing at 1250°C (blue pattern), as-sprayed SPS-$Al_2O_3$ coating (black pattern) and as sprayed SHVOF-$Al_2O_3$ coating (orange pattern).*

After a certain critical amount of alumina reaches in the melt, anorthite was re-precipitated, as previously observed [14] (blue dashed arrow). Contrary, in the current study, due to a higher CaO content of the CMAS (red circle), the melt composition moved towards the line where both anorthite and gehlenite were re-precipitated (red arrow).

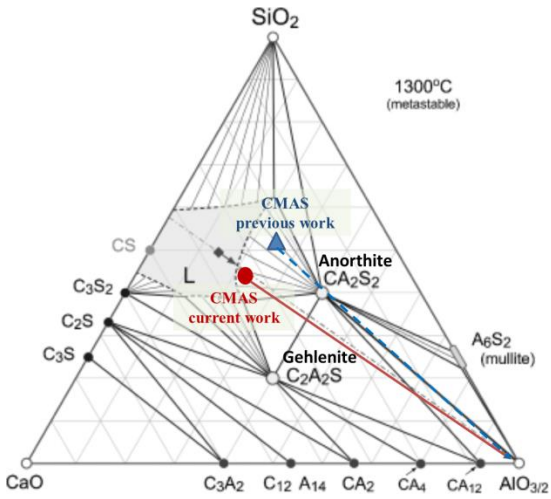


*Figure 7: Ternary phase diagram $AlO_{1.5}$-$SiO_2$-CaO, metastable isothermal cross section at 1300°C [19] based on [20] (Fig. 630), the relative CMAS composition used in this study (red dot) and in [14] (blue triangle), arrows indicating the composition of each CMAS with increasing $Al_2O_3$.*

**Reaction Layers and Products**

Comparing the SEM-micrographs of the infiltrated SPS and SHVOF layers in Fig. 2 and Fig. 3, it can be seen that uniform reaction layers were only formed on top of the SHVOF-$Al_2O_3$ coating. They consisted mainly of the reaction product Al-Mg-Fe-spinel and a reaction front which were indicated between the two dashed lines in Fig. 2d and 3d; their compositions estimated by EDS spot measurements are given in Table 2. The thicknesses of the reaction layers were found to be in between 0.5 - 1.5 µm after 5 min @ 1250°C (Fig. 2d) and 2.7 - 3.2 µm after 5 h @ 1250 °C (Fig. 3d). These thicknesses were considerably thinner compared to the reaction layer thickness of EB-PVD-$Al_2O_3$ observed in the previous work [14], where the reaction layer had a thickness of 2 µm after 5 min and 8.5 µm after 5 h infiltration. However, it should be noted that this variation in the reaction layer thickness was not necessarily to be linked to the influence of different coating methods (SHVOF vs. EB-PVD) but also to the different chemical composition of the CMAS used in these two cases. The CMAS deposit used in this study has a higher CaO content than for the EB-PVD layer [14].

Figures 2b and 2d (SPS) and Figures 3b and 3d (SHVOF) show high-magnification SEM micrographs of the reaction zones of the infiltrated samples. The local oxides composition (mol.-%) obtained by EDS spot measurements at these zones are given in Table 2.

The phases are identified by combining the peaks identified in XRD analysis of the powder mixture with the chemical composition of a specific phase in the cross sectional SEM image via EDS spot measurement. As these reaction phases have a broad range of stoichiometry, the actual composition measured via EDS can slightly differ from the stoichiometry identified in the XRD patterns.

The following reaction products were formed during infiltration tests:

- Anorthite ($CaAl_2Si_2O_8$) phase was formed in all the studied cases. Its composition has changed slightly with respect to the time especially in $Al_2O_3$ and CaO contents. Furthermore, small contents of MgO and FeO were found within it for both 5 min and 5 h, as shown in Table 2. Pure anorthite only contains $Al_2O_3$, CaO and $SiO_2$ however a limited solubility of MgO and FeO is still possible. With longer annealing time the fraction of these two oxides decreased. It probably diffused out of the anorthite grains and immigrated into the residue:
- Spinel ($MgAl_{2-x}Fe_xO_4$) formed only in the SHVOF-layer after 5 h infiltration. This phase was identified at the interface between the $Al_2O_3$ coating and the CMAS, with a layer of anorthite separating it from the deposit (Fig. 3d). Between the anorthite and spinel, a reaction front was found which consists of MgO and FeO, but also still $SiO_2$ and CaO in concentrations of 5 to 7 mol.-%. Spinel peaks were also identified in the XRD pattern of the $Al_2O_3$-CMAS-powder mixture (Fig 6). $MgAl_2O_4$ (spinel) is generally found when $Al_2O_3$ reacts with CMAS, as reported in literature [12, 14].

Two other phases were found only in the SPS $Al_2O_3$ coatings after 5 h infiltration: gehlenite ($Ca_2Al_2SiO_7$) and a "needle-like" structure phase (see high-magnification SEM-micrograph of Fig. 3b), containing mainly $Al_2O_3$ $SiO_2$ and CaO, as well as MgO, FeO and $TiO_2$ (between 1.9 and 6.0 mol.-%). The precise determination of the chemical composition with EDS-spot measurement of this "needle-phase" is quite difficult because of its smaller size. The X-ray signals used for EDS-measurements come from an area that is at least 1 µm in diameter and around 1.5 µm depth.

*Table 2: Chemical composition of reaction products in the infiltrated $Al_2O_3$ suspension sprayed coatings, estimated by EDS spot measurements.*

| Possible phase | Phase abbreviation | $Al_2O_3$ Coating / Infiltration time | Chemical composition [mol.-%] estimated by EDS spot measurements | | | | | |
|---|---|---|---|---|---|---|---|---|
| | | | $AlO_{1,5}$ | $SiO_2$ | CaO | MgO | FeO | $TiO_2$ |
| Anorthite | An | SPS / 5 min | 42.1 | 35.5 | 18.5 | 1.3 | 2.7 | |
| Anorthite | An | SPS / 5 h | 39.7 | 38.2 | 20.6 | 0.6 | 0.9 | |
| Anorthite | An | SHVOF / 5 h | 35.6 | 39.0 | 24.4 | | 1.0 | |
| Anorthite | An | | 35.8 | 37.8 | 24.1 | 0.6 | 1.6 | |
| Gehlenite | Ge | SPS / 5 h | 39.9 | 19.9 | 36.3 | 2.1 | 1.9 | |
| Gehlenite | Ge | | 40.4 | 19.6 | 36.0 | 2.1 | 1.9 | |
| "Needle-like" phase | Needles | SPS / 5 h | 69.6 | 8.3 | 11.6 | 3.5 | 5.1 | 1.9 |
| "Needle-like" phase | Needles | | 71.5 | 6.1 | 10.4 | 3.7 | 6.0 | 2.2 |
| Spinel | Sp | SHVOF / 5 h | 77.2 | | | 18.1 | 4.8 | |
| " Reaction front" | Reac-f | | 60.5 | 7.3 | 5.0 | 21.5 | 5.6 | |
| CMAS/residue | CMAS | SPS / 5 min | 21.3 | 31.7 | 33.8 | 4.7 | 6.6 | 1.9 |
| CMAS/Residue | CMAS | SPS / 5 h | 44.1 | 14.8 | 14.8 | 9.5 | 15.9 | 0.9 |
| CMAS/Residue | CMAS | SHVOF / 5 h | 18.8 | 36.9 | 31.8 | 9.1 | 2.1 | 1.3 |

As the needles are embedded in anorthite, the contents of MgO, FeO and $TiO_2$ could be probably much higher. In order to identify this "needle-like" structure phase, TEM examinations are necessary. The formation of this phase is linked probably to the specific microstructure that causes a certain relation of the available $Al_2O_3$ from the coating and the available molten CMAS.

A clear difference in the reaction products were observed between alumina-CMAS powder mixture (reaction products identified by XRD analysis), and infiltrated SPS-$Al_2O_3$ and SHVOF-$Al_2O_3$ coatings (reaction products determined by EDS analysis) It reveals the fact that the coating microstructure played a key role in defining the reaction products by influencing the solvent-solute-ratio. In the infiltration experiments, alumina coating reacted / dissolved into the infiltrated CMAS and enriched with extra alumina. With increasing infiltration time, the chemical composition of the CMAS has changed significantly due to the alumina diffusion from the coating into the melt. This change in melt composition depended on how much solvent (the CMAS melt) was available in relation to the solute (here alumina or other already precipitated phases).
In case of the powder mixture, solvent and solute were well mixed, with a slight excess of CMAS concentration. This allowed the formation of anorthite, but also gehlenite and spinel which ensured enough solute/solvent ratios for the reaction products.

In case of the SPS coating, the melt infiltrated into the small pores and was surrounded by enough alumina coating. Hence local composition changed into anorthite crystals phase once the melt cooled down. Gehlenite was formed only after the 5 h infiltration and merely in larger gaps. Gehlenite formation seemed to require less alumina than anorthite and more CaO; once the melt forms anorthite, the rest glass which contains all the other oxides would crystallize into gehlenite phase upon slow isothermal cooling. As previously mentioned, the 5 min infiltration tests contain quick quenching, whereas the 5 h experiments were slowly, isothermally cooled (10 K/min) which would allow the separation of phases. That can be the main reason for the absence of Gehlenite phase in case of the 5 min experiment. $TiO_2$ and FeO appeared in the "needle-like phases (Table 2) of SPS infiltrated for 5 h @ 1250 °C. The absence of $TiO_2$ in both anorthite and gehlenite and higher presence of FeO in needle-like phase can be pointed out from Table 2. It is known from literature that $TiO_2$ reacts with FeO to form pseudobrookite (Ps). As we see from the needle-like phase in case of SPS alumina after 5 h, there exists a tendency that $TiO_2$ –FeO rich phase containing all other elements would form pseudobrookite upon long-term annealing.

Spinel formation in case of dense SHVOF-coating was a direct evidence of coating microstructure influence, where dense alumina offers resistance to the CMAS infiltration and allowed enough time which triggers the reaction with FeO and MgO. Thus, more solvent was available in this case.

## Conclusions

From the performed experiments following conclusions can be drawn:

- $Al_2O_3$ sprayed coatings with defined coating microstructures and porosity levels were produced by two different suspension spraying methods on top of EB-PVD 7YSZ layers. Porous alumina coatings with about 30 % porosity were obtained by SPS, whereas a very dense structure with porosity content below 4 % was obtained by SHVOF. The presence of some through thickness cracks in the coating was observed in SHVOF coating.
- The coating microstructures strongly influenced the infiltration behavior of the CMAS melt. Highly porous SPS alumina coatings were infiltrated faster and have reacted stronger as they offer a higher specific contact surface area with the CMAS; thus the SPS coatings resulted in low resistance against CMAS infiltration. After 5 min infiltration at 1250 °C SPS alumina coating was almost completely infiltrated, whereas in SHVOF $Al_2O_3$ coating only a few µm were infiltrated in the crack-free sections.

• The SHVOF-coatings have shown a promising CMAS sealing behavior, although the characteristic thickness through cracks have proven to be weak areas and allowed CMAS infiltration. However, a uniform thin Fe-Mg-Al spinel layer has formed on the coating and acted as a barrier against CMAS infiltration.

• A clear influence of the coating microstructure on the infiltration reaction products was observed. Different reaction products other than spinel were formed in both SPS and SHVOF coatings namely anorthite, gehlenite, as well as "needle-like" phases which consists of $Al_2O_3$, CaO, $SiO_2$ and FeO as main components. However, these phases have not exhibited protective nature against CMAS infiltration.

SHVOF $Al_2O_3$ coating is a promising candidate as a sacrificial coating due to its slow-growing uniform reaction zone that inhibits further CMAS infiltration. However, further optimization of the coating process is needed to improve the consistency of the coating when exposed to CMAS mitigation and elevated temperatures.

## Acknowledgments

The authors express their gratitude to J. Brien, A. Handwerk and D. Peters from DLR for producing of the EB-PVD 7YSZ layers, as well as for technical support and advisory.
The work was performed in the Framework of the Research Project DFG No. SCHU 1372/5 1, LE1373/34-1 funded by DFG-Deutsche Forschungsgemeinschaft (German Science Foundation). The authors acknowledge the financial support.

## References

1. D.R. Clarke, *et al*., "Thermal-barrier coatings for more efficient gas-turbine engines", *MRS Bull.* Vol. 37, No. 10 (2012), p 891–898
2. C.G. Levi "Emerging materials and processes for thermal barrier systems", *Curr. Opin. Solid State Mater. Sci.*, Vol.8, No. 1 (2004), p 77–91
3. A.F. Renteria, *et al.*, "Effect of morphology on thermal conductivity of EB-PVD PYSZ TBCs*", Surf. Coat. Technol*., Vol. 201 (2006), p 2611–2620.
4. S. Sampath, *et al.*, "Processing science of advanced thermal-barrier systems", *MRS Bull.*, Vol. 37 (2012), p 903–910
5. R. Naraparaju, *et al.*, "Degradation study of 7wt. % yttria stabilized zirconia (7YSZ) thermal barrier coatings on aero-engine combustion chamber parts due to infiltration by different CaO-MgO-$Al_2O_3$-$SiO_2$ variants", *Surf. Coat. Technol*., 260 (2014), p 73–81.
6. R. Naraparaju, *et al.*, "Tailoring the EB-PVD columnar microstructure to mitigate the infiltration of CMAS in 7YSZ thermal barrier coatings", *J. Eur. Ceram. Soc.* Vol. 37 No. 1 (2017) p. 261–270.
7. R. Naraparaju, *et al.*, "The Accelerating Effect of $CaSO_4$ within CMAS (CaO–MgO–$Al_2O_3$–$SiO_2$) and its Effect on the Infiltration Behavior in EB-PVD 7YSZ," *J. Am. Ceram. Soc.*, Vol. 99 (2016), p 1398-1403
8. S. Krämer, *et al.*, "Infiltration-inhibiting reaction of gadolinium zirconate thermal barrier coatings with CMAS melts", *J. Am. Ceram. Soc.* Vol. 91 (2008), p 576–583
9. R. Naraparaju, *et al.*, "Interaction and infiltration behavior of Eyjafjallajökull, Sakurajima volcanic ashes and a synthetic CMAS containing FeO with/in EB-PVD $ZrO_2$-65 wt.%$Y_2O_3$ coating at high temperature", *Acta Mater.*, Vol. 136 (2017), p 164–180
10. U. Schulz, *et al.*, "Degradation of $La_2Zr_2O_7$ and other novel EB-PVD thermal barrier coatings by CMAS (CaO-MgO-$Al_2O_3$-$SiO_2$) and volcanic ash deposits", *Surf. Coat. Technol*., Vol. 235 (2013), p 165–173
11. A.K. Rai, *et al.*, "CMAS resistant thermal barrier coatings (TBC)", *Int. J. Appl. Ceram. Technol.*, Vol. 7 (2010) p 662–674
12. X.-f. Zhang, *et al.*, "In situ synthesis of α-alumina layer on thermal barrier coating for protection against CMAS (CaO–MgO–$Al_2O_3$–$SiO_2$) corrosion", *Surf. Coat. Technol.*, Vol. 261 (2015) p 54–59
13. P. Mohan, *et al.*, "Electrophoretically deposited alumina as protective overlay for thermal barrier coatings against CMAS degradation", *Surf. Coat. Technol.*, Vol. 204 (2009) p.797–801
14. R. Naraparaju, *et al*, "EB-PVD alumina ($Al_2O_3$) as a top coat on 7YSZ TBCs against CMAS/VA infiltration: Deposition and reaction mechanisms" *J. Eur. Ceram. Soc.* Vol. 38 (2017), p. 3333-3346
15. L.-M. Berger, *et al.*, "Thermal Spraying with Suspensions: an Economic Spray Process", *Therm. Spray Bull.*, Vol. 6 (2), (2013), p 98-101
16. F.-L. Toma, *et al.*, "Demands, Potentials, and Economic Aspects of Thermal Spraying with Suspensions: A Critical Review", *J. Therm. Spray Technol.*, Vol. 24 (7), (2015), p 1143-1152
17. A. Potthoff, *et al.*, "Development and Application of Binary Suspensions in the Ternary System $Cr_2O_3$-$TiO_2$-$Al_2O_3$ for S-HVOF Spraying", *J. Therm. Spray Technol.*, Vol. 27, (2018), p 1143-1152
18. M. Barbosa, *et al.*, "Suspension Sprayed YSZ Thermal Barrier Coatings: Road to Industrial Application", *ITSC 2018—Proceed. Intern. Therm. Spray Conf*. May 7-10, 2018, Orlando, Florida, USA, F. Azarmi, K. Balani, T. Eden, T. Hussain, Y.-C. Lau, H. Li, K. Shinoda, F.-L. Toma, J. Veilleux, (Eds), ASM Int. 2018, p 113- 119
19. S. Krämer, *et al.*, "Thermochemical Interaction of Thermal Barrier Coatings with Molten CaO–MgO–$Al_2O_3$–$SiO_2$ (CMAS) Deposits", *J. Am. Ceram. Soc.*, Vol. 89 (2006), p 3167-3175
20. E. M. Levin, *et al.*, *Phase Diagrams for Ceramists*, The American Ceramic Society (Columbus, OH, 1964) p 210, 219, 246.